

# High spectral resolution observations of HNC<sub>3</sub> and HCCNC in the L1544 prestellar core

C. Vastel<sup>1</sup>★, K. Kawaguchi<sup>2</sup>, D. Quénard<sup>3</sup>, M. Ohishi<sup>4</sup>, B. Lefloch<sup>5</sup>, R. Bachiller<sup>6</sup>, H. S. P. Müller<sup>7</sup>†

<sup>1</sup>IRAP, Université de Toulouse, CNRS, UPS, CNES, Toulouse, France

<sup>2</sup>Graduate School of National Science and Technology, Okayama University, 3-1-1 Tsushima-naka, Okayama 700-8530, Japan

<sup>3</sup>School of Physics and Astronomy, Queen Mary University of London, Mile End Road, London E1 4NS, UK

<sup>4</sup>Astronomy Data Center, National Astronomical Observatory of Japan, 2-21-1 Osawa, Mitaka, Tokyo 181-8588, Japan

<sup>5</sup>Université de Grenoble Alpes, CNRS, IPAG, 38000 Grenoble, France

<sup>6</sup>Observatorio Astronómico Nacional (OAN, IGN), Calle Alfonso XII, 3, 28014 Madrid, Spain

<sup>7</sup>I. Physikalisches Institut, Universität zu Köln, Zùlpicher Str. 77, 50937 Köln, Germany

Accepted 2017 November 27. Received 2017 November 21; in original form 2017 October 21

## ABSTRACT

HCCNC and HNC<sub>3</sub> are less commonly found isomers of cyanoacetylene, HC<sub>3</sub>N, a molecule that is widely found in diverse astronomical sources. We want to know if HNC<sub>3</sub> is present in sources other than the dark cloud TMC-1 and how its abundance is relative to that of related molecules. We used the ASAI unbiased spectral survey at IRAM 30m towards the prototypical prestellar core L1544 to search for HNC<sub>3</sub> and HCCNC which are by-product of the HC<sub>3</sub>NH<sup>+</sup> recombination, previously detected in this source. We performed a combined analysis of published HNC<sub>3</sub> microwave rest frequencies with thus far unpublished millimeter data because of issues with available rest frequency predictions. We determined new spectroscopic parameters for HNC<sub>3</sub>, produced new predictions and detected it towards L1544. We used a gas-grain chemical modelling to predict the abundances of N-species and compare with the observations. The modelled abundances are consistent with the observations, considering a late stage of the evolution of the prestellar core. However the calculated abundance of HNC<sub>3</sub> was found 5–10 times higher than the observed one. The HC<sub>3</sub>N, HNC<sub>3</sub> and HCCNC versus HC<sub>3</sub>NH<sup>+</sup> ratios are compared in the TMC-1 dark cloud and the L1544 prestellar core.

**Key words:** astrochemistry—line: identification—ISM: abundances—ISM: molecules—ISM: individual objects (L1544)

## 1 INTRODUCTION

Given their powerful diagnostic ability, several unbiased spectral surveys have been obtained in the past few years in the millimeter and sub-millimeter bands accessible from the ground obtained in the direction of star forming regions (e.g. Herbst 2009). By far the most targeted sources are hot cores, the regions of high mass protostars formation, where the dust temperature exceeds the sublimation temperature of the water-ice grain mantles, ~100 K. So far, unbiased spectral surveys of low-mass solar type objects on a wide frequency range have been carried out in IRAS 16293-2422 (Blake et al. 1994; Caux et al. 2011; Jørgensen et al. 2016). The increased capabilities of the IRAM 30 m telescope make access to a new level in the investigation of molecular complexity in star-forming regions with the ASAI (Astrochemi-

cal Studies At IRAM) Large program (see Lefloch et al. 2017 for a review) in the millimeter regime (project number 012-12). One of the targeted sources is the prototypical prestellar core, L1544, located in the Taurus molecular cloud complex (d ~140 pc). This source is characterised by a high central density ( $\geq 10^6$  cm<sup>-3</sup>), a low temperature ( $\leq 10$  K), a high CO depletion and a large degree of molecular deuteration (Crapsi et al. 2005; Vastel et al. 2006; Spezzano et al. 2013). The study of the many tracers detected in this source led to the reconstruction of its physical and dynamical structure (Keto et al. 2014). This core is also famous for being the first prestellar core where water has been detected (Caselli et al. 2012) and its line profile, characteristic of gravitational contraction, is confirming that L1544 is on the verge of the collapse. The ASAI high spectral resolution and high sensitivity (average rms of ~4mK in a 50 kHz frequency bin) led to many discoveries. For example, we have been able to obtain a full census of oxygen-bearing iCOMs (interstellar complex organic molecules), and it was found that a

★ E-mail: cvastel@irap.omp.eu

† E-mail: hspm@ph1.uni-koeln.de

non-thermal desorption mechanism is possibly responsible for the observed emission of methanol and COMs from the same external layer (Vastel et al. 2014). The detection of the cyanomethyl radical ( $\text{CH}_2\text{CN}$ ) for the first time in a prestellar core was reported by Vastel et al. (2015b) who were able to identify resolved hyperfine transitions of the *ortho* and *para* forms from the calculated frequencies. Finally, protonated cyanides, such as  $\text{HCNH}^+$  and  $\text{HC}_3\text{NH}^+$ , have also been detected for the first time in a prestellar core (Quénard et al. 2017). The high spectral resolution of the observations allows to resolve the hyperfine structure of  $\text{HCNH}^+$ . The study of some nitrogen species linked to their production ( $\text{HCN}$ ,  $\text{HNC}$ ,  $\text{HC}_3\text{N}$ ) coupled with a gas-grain chemical modelling shows that the emission of these ions originates in the external layer where non-thermal desorption of other species was previously observed.

In the present study we report on the detection of the  $\text{HNC}_3$  species for the first time in a prestellar core using the ASAI IRAM-30m spectral survey. We also report the detection of 4 transitions of  $\text{HCCNC}$ , one of them being already detected in the same source by Jiménez-Serra et al. (2016). The first astronomical detections of  $\text{HCCNC}$  and  $\text{HNC}_3$  were reported by Kawaguchi et al. (1992a) and Kawaguchi et al. (1992b), respectively, towards a cold, dark molecular cloud, TMC-1. These molecules are linked to the chemistry of  $\text{HC}_3\text{NH}^+$ , previously detected in the ASAI observations. The observed line frequencies associated with  $\text{HNC}_3$  were slightly off ( $\sim 0.2$  MHz) compared to the theoretical prediction given by the JPL catalog (Pickett et al. 1998). We present in this letter the analysis of  $\text{HNC}_3$  published microwave frequencies with millimeter data, up to 300 GHz.

## 2 LABORATORY SPECTROSCOPIC CONSIDERATIONS

Rest frequency predictions for the linear isocyanoacetylene ( $\text{HCCNC}$ ) molecule were taken from the JPL catalog. The entry is based on Fourier transform microwave (FTMW) and millimeter-wave (mmW) measurements (Krüger et al. 1991; Guarnieri et al. 1992), the dipole moment was determined by Krüger et al. (1993).

Iminopropadienyldiene ( $\text{HNC}_3$ ) is a quasi-linear molecule, i.e., an asymmetric top rotor with a low barrier to linearity (Botschwina 2003) such that rotational levels with  $K_a \geq 1$  will be difficult to be observed in the laboratory, even less so in the ISM. The initial predictions for  $\text{HNC}_3$  were also taken from the JPL catalog. The entry was based on FTMW data (Hirahara et al. 1993) and additional frequencies from the radio astronomical observations (Kawaguchi et al. 1992b). We were able to tentatively assign emission lines for this species in our L1544 ASAI spectral survey. However, the predictions deviated significantly (between about 170 and 280 kHz) from our observed lines because the data employed for the initial predictions extended only to 47 GHz. Kawaguchi et al. (1992b) mentioned mmW laboratory measurements of  $\text{HNC}_3$  and published resulting spectroscopic parameters, but not the rest frequencies with their uncertainties. In the present study we combine FTMW data (Hirahara et al. 1993) displaying  $^{14}\text{N}$  hyperfine structure (HFS) splitting with the mmW laboratory data without HFS splitting

to obtain improved spectroscopic parameters; one poorly fitting weak FTMW transition frequency was omitted. The resulting parameters are shown in Table 1. Table A1 (online supplementary material) summarized experimental lines with uncertainties and residuals between measured rest-frequency and that calculated from the final spectroscopic parameters along with predictions up to 50 GHz under consideration of HFS splitting. Table A2 presents the corresponding data without HFS splitting up to 300 GHz. A dipole moment of 5.665 D was calculated by Botschwina et al. (1992). The predictions and associated files will be available in the CDMS (Endres et al. 2016).

**Table 1.** Spectroscopic parameters (MHz) of iminopropadienyldiene ( $\text{HNC}_3$ ). Numbers in parentheses are one standard deviation in units of the least significant digits.

| Parameter       | Value           |
|-----------------|-----------------|
| $B$             | 4668.33576 (39) |
| $D \times 10^6$ | 618.57 (28)     |
| $eQq$           | 1.0875 (64)     |

## 3 OBSERVATIONS AND RESULTS

All the informations concerning the observations performed at the IRAM 30m can be found in Vastel et al. (2014) and Quénard et al. (2017). Table 2 reports the spectroscopic parameters and the properties of the detected lines, obtained by a gaussian fitting function. For the line identification, we used the CASSIS<sup>1</sup> software (Vastel et al. 2015a). We present in Figure 1 the three  $\text{HNC}_3$  transitions and in Figure 2 the four  $\text{HCCNC}$  transitions, detected in the ASAI spectral survey. Note that the 10–9  $\text{HCCNC}$  transition has also been detected by Jiménez-Serra et al. (2016). Both species, as well as  $\text{HC}_3\text{N}$  already presented in Quénard et al. (2017) are produced through the  $\text{HC}_3\text{NH}^+$  recombination reaction. This ion has previously been detected in L1544 by Quénard et al. (2017). Local thermodynamic equilibrium (LTE) analysis of  $\text{HC}_3\text{NH}^+$  leads to a derived column density of  $(1\text{--}2) \times 10^{11} \text{ cm}^{-2}$ . In the case of  $\text{HC}_3\text{N}$  a non-LTE analysis leads to the computation of a column density of  $(1.6\text{--}2.4) \times 10^{13} \text{ cm}^{-2}$ .

The vertical dashed line in Figure 2 represents the velocity in the Local Standard of Rest ( $V_{LSR}$ ) of  $7.2 \text{ km s}^{-1}$  for the  $\text{HCCNC}$  species showing a good match (within  $0.1 \text{ km s}^{-1}$ ) between the observed frequencies and the calculated frequencies quoted by the JPL archive database (Pickett et al. 1998). However, the  $\text{HNC}_3$  fitted frequencies from the JPL database cannot be reproduced with the L1544  $V_{LSR}$ , with an observed shift of about  $1 \text{ km s}^{-1}$ . We therefore use the frequencies as computed in Section 2 (see Table A2). In the absence of collisional coefficients for  $\text{HNC}_3$  and  $\text{HCCNC}$ , LTE analysis has been performed using CASSIS, assuming no beam dilution. Note that LTE and non-LTE analysis for  $\text{HC}_3\text{N}$  led similar results and we can only assume it will be the same for  $\text{HNC}_3$  and

<sup>1</sup> <http://cassis.irap.omp.eu>

**Table 2.** Properties of the observed HNC<sub>3</sub> and HCCNC ( $E_{\text{up}} \leq 30$  K,  $A_{\text{ul}} \geq 5 \times 10^{-6} \text{ s}^{-1}$ ) lines. Note that the errors in the integrated intensities include the statistical uncertainties from the gaussian fits of the lines. The rms has been computed over 20 km s<sup>-1</sup>.

| HNC <sub>3</sub>              |                         |                        |                                       |                               |   |             |
|-------------------------------|-------------------------|------------------------|---------------------------------------|-------------------------------|---|-------------|
| Transitions<br>( $J' - J''$ ) | Rest Frequency<br>(MHz) | $E_{\text{up}}$<br>(K) | $A_{\text{ul}}$<br>(s <sup>-1</sup> ) | FWHM<br>(km s <sup>-1</sup> ) | $\int T_{\text{mb}} dV$<br>(mK km s <sup>-1</sup> ) | rms<br>(mK) |
| 8 – 7                         | 74692.1053              | 16.13                  | $7.32 \times 10^{-5}$                 | $0.57 \pm 0.05$               | $31.8 \pm 5.6$                                      | 4.8         |
| 9 – 8                         | 84028.2399              | 20.16                  | $1.05 \times 10^{-4}$                 | $0.34 \pm 0.08$               | $9.5 \pm 4$   | 4.5         |
| 10 – 9                        | 93364.2409              | 24.64                  | $1.45 \times 10^{-4}$                 | $0.51 \pm 0.07$               | $7.6 \pm 2$   | 2.7         |
| HCCNC                         |                         |                        |                                       |                               |   |             |
| 8 – 7                         | 79484.1277              | 17.17                  | $2.36 \times 10^{-5}$                 | $0.41 \pm 0.01$               | $73.4 \pm 2.3$                                      | 4.3         |
| 9 – 8                         | 89419.2601              | 21.46                  | $3.34 \times 10^{-5}$                 | $0.37 \pm 0.04$               | $44.0 \pm 9.1$                                      | 2.7         |
| 10 – 9                        | 99354.2570              | 26.23                  | $4.62 \times 10^{-5}$                 | $0.44 \pm 0.03$               | $29.2 \pm 4.1$                                      | 2.5         |
| 11 – 10                       | 109289.1036             | 31.47                  | $6.19 \times 10^{-5}$                 | $0.45 \pm 0.07$               | $11.7 \pm 3.5$                                      | 3.8         |

HCCNC. The best LTE fit is obtained for a low excitation temperature of (6–8) K with column densities of  $(0.75\text{--}2) \times 10^{11} \text{ cm}^{-2}$  for HNC<sub>3</sub> and  $(0.85\text{--}2.2) \times 10^{12} \text{ cm}^{-2}$  for HCCNC. Jiménez-Serra et al. (2016) estimated an observed column density of  $(0.3\text{--}3.0) \times 10^{12} \text{ cm}^{-2}$  in a (5–10) K range using one transition only. In any case, the observed HCCNC column density is  $\sim 10$  times higher than HNC<sub>3</sub>.

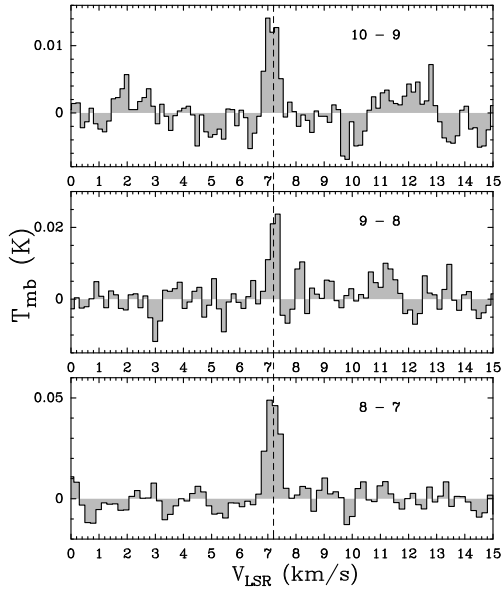


**Figure 1.** Three detected transitions of HNC<sub>3</sub> towards L1544. The vertical line show a  $V_{\text{LSR}} = 7.2 \text{ km s}^{-1}$ .

#### 4 CHEMICAL MODELLING

Using a gas-grain chemical code (Nautilus, described in Ruaud et al. 2016), Quénard et al. (2017) calculated the predicted abundance using a two-step model by varying the initial gas densities of the initial phase. The resulting abundances have been compared to the observed column densities and models with an age  $\geq 10^5$  years give a satisfactory agreement to the observations. The same modelling shows that HC<sub>3</sub>NH<sup>+</sup>, as well as HC<sub>3</sub>N and HNC<sub>3</sub> are emitted mostly

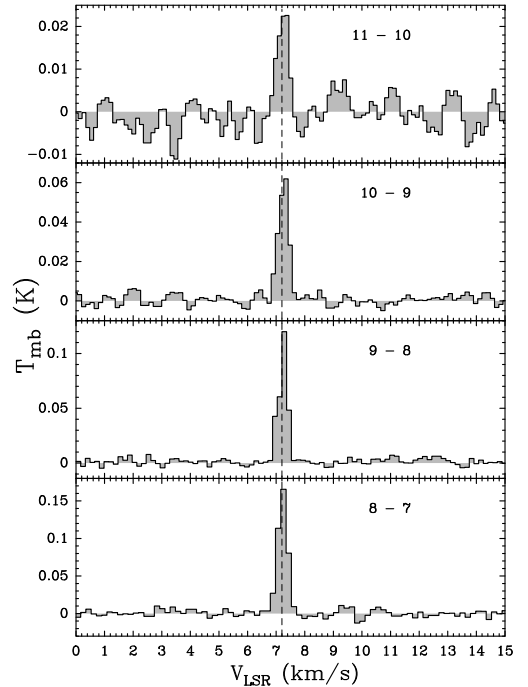
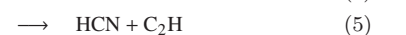


**Figure 2.** Four detected transitions of HCCNC towards L1544. The vertical line show a  $V_{\text{LSR}} = 7.2 \text{ km s}^{-1}$ .

in an external layer at about  $10^4$  au from the center, with a temperature of about 10 K and a density of  $\sim 10^4 \text{ cm}^{-3}$ . When HC<sub>3</sub>NH<sup>+</sup> recombines with an electron, the neutralized HC<sub>3</sub>NH molecule has a substantial internal energy, leading to the breaking of chemical bonds. HC<sub>3</sub>N, HNC<sub>3</sub> and HCCNC are all products of the HC<sub>3</sub>NH<sup>+</sup> dissociative recombination (DR) reaction:



Reactions (5) and (6) are not the main routes for the production of HCN and HNC, which are also products of the DR of HCNH<sup>+</sup>. Also, the DR of HC<sub>3</sub>NH<sup>+</sup> is not the main

route for the production of HC<sub>3</sub>N. In their theoretical analysis, Osamura et al. (1999) have chosen equal branching fractions for reactions (1) and (2) that are 5 times greater than those for the products in reactions (3) and (4). They also concluded that a variation from 3 to 9 (instead of 5) do not have a major effect on the calculated abundances of the metastable isomers of HC<sub>3</sub>N. The branching ratio for the DR of DC<sub>3</sub>ND<sup>+</sup> have been estimated using the heavy ion storage ring CRYRING in Stockholm, Sweden (Vigren et al. 2012) which would, in analogy with HC<sub>3</sub>NH<sup>+</sup> lead to the following branching fractions: 22%, 22%, 4%, 4%, 24%, 24% for reactions (1), (2), (3), (4), (5) and (6) respectively. The thermal rate coefficients for the DR of the DC<sub>3</sub>ND<sup>+</sup> has been measured by Geppert et al. (2004):  $1.5 \times 10^{-6} (\text{T}/300)^{-0.58} \text{ cm}^3 \text{ s}^{-1}$ . We used the KIDA database (<http://kida.obs.u-bordeaux1.fr/>) and modified the HC<sub>3</sub>NH<sup>+</sup> dissociative reaction rate according to Geppert et al. (2004), using the branching ratio following Vigren et al. (2012).

Figure B1 (online supplementary material) shows the results of the chemical modelling for the HCNH<sup>+</sup> and HC<sub>3</sub>NH<sup>+</sup> ions using the modified network described above as was performed in Quénard et al. (2017). The model is divided into two phases. The first phase corresponds to the evolution of the chemistry in a diffuse or molecular cloud (hereafter ambient cloud) and depends on the assumed initial H density. The chemical composition then evolves for 10<sup>6</sup> years. The abundances from this first step are then used as initial abundances for the second step where we consider the physical structure of the L1544 prestellar core (Keto et al. 2014). The HCNH<sup>+</sup> and HC<sub>3</sub>NH<sup>+</sup> species are emitted from the outer layer when non-thermal desorption of other species was previously observed (Vastel et al. 2014). Solutions 1, 2 and 3 (grey box in Fig. B1) represent the best comparison with the observation for the HCNH<sup>+</sup> ion (see Table 2–4 from Quénard et al. (2017)). The present modelling shows that the HC<sub>3</sub>NH<sup>+</sup> observations are better reproduced with the new recombination rate, compared to Quénard et al. (2017), by a factor of ~ 10. We also present in Fig. 3 the comparison between the modelling and the observed column densities of HCCNC, HC<sub>3</sub>N and HNC<sub>3</sub>. The HCCNC modelling is compatible with solution 1 which represent the low-metal initial abundances while HNC<sub>3</sub> is higher by a factor 5-10 compared to the observations. This solution has already been obtained for HC<sub>3</sub>NH<sup>+</sup>, HC<sub>3</sub>N as well as other nitrogen species which have already been published by Quénard et al. (2017). We want to emphasise that, in the present network, the production of HNC<sub>3</sub> is dominated by the HC<sub>3</sub>NH<sup>+</sup> DR while the production of HC<sub>3</sub>N is dominated by the following reactions: C<sub>2</sub>H<sub>2</sub> + CN and CH<sub>2</sub>CCH + N. The network seems to over-produce HNC<sub>3</sub> compared to the observations. We present in Fig. B2 the comparison for the HNC<sub>3</sub> species between the chemical modelling presented in Quénard et al. (2017) and the present modified network. The destruction pathway for HNC<sub>3</sub> is dominated by the electron recombination for which the rate is only estimated following the experimental dissociative attachment of HNO<sub>3</sub> (Adams et al. 1986; Harada & Herbst 2008). Note also that the branching ratios for reactions (1)–(6) are highly uncertain, so a variation could have an impact on the chemical modelling of the aforementioned species. Note also that the HNC<sub>3</sub>, HC<sub>3</sub>N and HCCNC molecules may be produced from the linear HCCNCH<sup>+</sup> ion for which we have no spectroscopic information so far.

## 5 COMPARISON WITH THE TMC-1 DARK CLOUD

HC<sub>3</sub>NH<sup>+</sup> (2 transitions), HNC<sub>3</sub> (3 transitions) and HCCNC (3 transitions) have been detected for the first time in the cold starless cloud TMC-1 (position of maximum cyanopolyne emission:  $\alpha(2000) = 04^{\text{h}}41^{\text{m}}42.47^{\text{s}}$ ,  $\delta(2000) = +25^{\circ}41'27.1''$ ) using the Nobeyama 45 m telescope (Kawaguchi et al. 1992a,b, 1994). Table 3 shows the comparison between the TMC-1 dark cloud and the L1544 prestellar core for the observations of these related species. The TMC-1 dark cloud is at an earlier stage than the L1544 prestellar core which is believed to be on the verge of collapse. It is important to note that, for TMC-1, the reported derived excitation temperatures for HC<sub>3</sub>NH<sup>+</sup>, HNC<sub>3</sub> and HCCNC are  $(6.5 \pm 0.1)$  K,  $(5.0 \pm 0.7)$  K and  $(6.4 \pm 0.6)$  K, respectively, at the lower end of the (6-8) K temperature range that we derived from the L1544 observations. The detection of the HC<sub>3</sub>N species has been reported for the first time in TMC-1 by Suzuki et al. (1992) who reported the column density to be  $1.71 \times 10^{14} \text{ cm}^{-2}$  using the J = 5–4 transition with the NRO 45-m telescope, if the excitation temperature is 6.5 K. Takano et al. (1998) then reported the analysis of the J = 2–1, 4–3, 5–4, and 10–9 transitions of HC<sub>3</sub>N at the 45-m Nobeyama telescope and derived a rotational temperature of  $(7.1 \pm 0.1)$  K and column density of  $(1.6 \pm 0.1) \times 10^{14} \text{ cm}^{-2}$ . The HC<sub>3</sub>N/HC<sub>3</sub>NH<sup>+</sup>, HNC<sub>3</sub>/HC<sub>3</sub>NH<sup>+</sup> and HCCNC/HC<sub>3</sub>NH<sup>+</sup> ratios in both sources are then similar, reflecting the cold and dense conditions in both environments:  $160 \pm 42$ ,  $0.4 \pm 0.1$  and  $2.9 \pm 0.8$  respectively for TMC-1, 80–240, 0.38–2, 4.25–22 respectively for L1544.

**Table 3.** Comparison of the observed column densities (in cm<sup>-2</sup>) between the TMC-1 dark cloud and the L1544 prestellar core.

|                                 | TMC-1  | L1544   |
|---------------------------------|--|---|
| HC <sub>3</sub> N               | $(1.6 \pm 0.1) \times 10^{14}$<br>Takano et al. (1998)     | $(1.6\text{--}2.4) \times 10^{13}$<br>Quénard et al. (2017) |
| HNC <sub>3</sub>                | $(3.8 \pm 0.6) \times 10^{11}$<br>Kawaguchi et al. (1992a) | $(0.75\text{--}2) \times 10^{11}$<br>this paper             |
| HCCNC                           | $(2.9 \pm 0.2) \times 10^{12}$<br>Kawaguchi et al. (1992b) | $(0.85\text{--}2.2) \times 10^{12}$<br>this paper           |
| HC <sub>3</sub> NH <sup>+</sup> | $(1.0 \pm 0.2) \times 10^{12}$<br>Kawaguchi et al. (1994)  | $(1\text{--}2) \times 10^{11}$<br>Quénard et al. (2017)     |

## 6 CONCLUSIONS

HNC<sub>3</sub> has been detected for the first time in a prestellar core, L1544. We computed its line frequencies, necessary for the line identification and estimation of the column density. We used a gas-grain chemical modelling and compared all related nitrogen species with the observations. Comparison of the observations with the model predictions suggests that the emission from HC<sub>3</sub>NH<sup>+</sup>, HC<sub>3</sub>N, HNC<sub>3</sub> and HCCNC originates in the outer layer where non-thermal desorption of other species was previously observed. We conclude that the modelled abundances are consistent with the observations, except for HNC<sub>3</sub>, considering a late stage of the evolution of the prestellar core, compatible with previous observations.

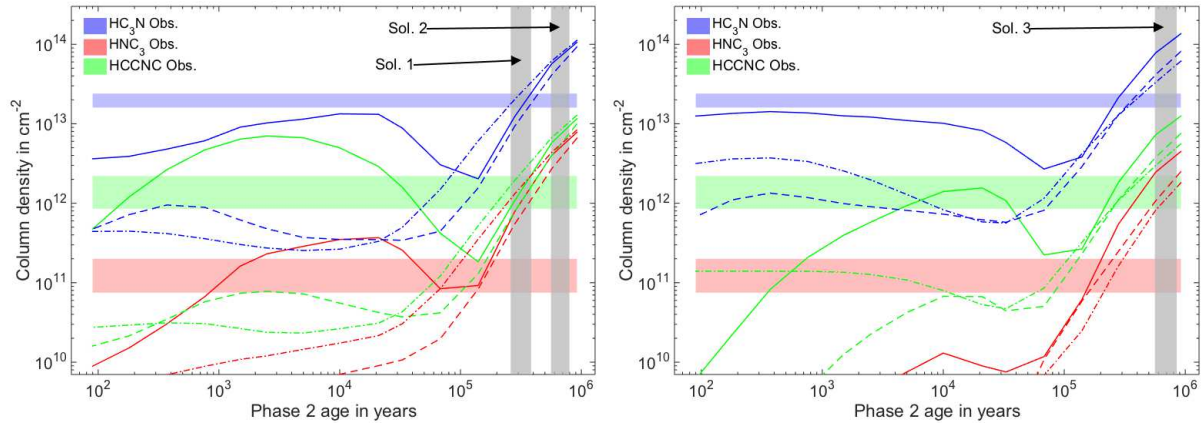


**Figure 3.** Column densities for  $\text{HC}_3\text{N}$ ,  $\text{HNC}_3$  and  $\text{HCCNC}$  as a function of the age of the phase 2 for different initial gas densities of the ambient cloud phase:  $10^2 \text{ cm}^{-3}$  (full line),  $3 \times 10^3 \text{ cm}^{-3}$  (dashed line), and  $2 \times 10^4 \text{ cm}^{-3}$  (dash-dotted line). The area of confidence of the observed column densities for these species is also shown. Grey areas shows the timespan area of confidence of each model based on the observed  $\text{HCNH}^+$ . These areas are labelled solutions 1, 2 and 3 (Quénard et al. 2017). *Left panel:* Model EA1 of initial atomic abundances (“low-metal abundances”). *Right panel:* Model EA2 of initial atomic abundances (“high-metal abundances”). All the informations on the modelling can be found in Quénard et al. (2017).

## ACKNOWLEDGEMENTS

Based on observations carried out with the IRAM 30 m Telescope. IRAM is supported by INSU/CNRS (France), MPG (Germany), and IGN (Spain). K.K. and M.O. are very grateful to S. Yamamoto and S. Saito for the opportunity to carry out laboratory spectroscopic investigations on  $\text{HNC}_3$  at the Nagoya University. H.S.P.M. thanks Y. Endo for comments on the FTMW data of  $\text{HNC}_3$ . M.O. is supported by the JSPS Kakenhi grant number JP15H03646. C.V. would like to thank J.-C. Loison for a fruitful discussion on the reaction rates and branching fraction of the DR of the  $\text{HC}_3\text{NH}^+$  ion. D.Q. acknowledges the financial support received from the STFC through an Ernest Rutherford Grant (proposal number ST/M004139).

## REFERENCES

- Adams N. G., Smith D., Viggiano A. A., Paulson J. F., Henchman M. J., 1986, *The Journal of Chemical Physics*, 84
- Blake G. A., van Dishoeck E. F., Jansen D. J., Groesbeck T. D., Mundy L. G., 1994, *The Astrophysical Journal*, 428, 680
- Botschwina P., 2003, *Phys. Chem. Chem. Phys.*, 5, 3337
- Botschwina P., Horn M., Seeger S., Flüge J., 1992, *Chemical Physics Letters*, 195, 427
- Caselli P., et al., 2012, *The Astrophysical Journal Letters*, 759, L37
- Caux E., et al., 2011, *Astronomy and Astrophysics*, 532, A23
- Crapsi A., Caselli P., Walmsley C. M., Myers P. C., Tafalla M., Lee C. W., Bourke T. L., 2005, *The Astrophysical Journal*, 619, 379
- Endres C. P., Schlemmer S., Schilke P., Stutzki J., Müller H. S. P., 2016, *J. Mol. Spectrosc.*, 327, 95
- Geppert W. D., et al., 2004, *The Astrophysical Journal*, 613, 1302
- Guarnieri A., Hinze R., Krüger M., Zerbe-Foese H., Lentz D., Preugschat D., 1992, *J. Mol. Spectrosc.*, 156, 39
- Harada N., Herbst E., 2008, *The Astrophysical Journal*, 685, 272
- Herbst E. & van Dishoeck E., 2009, *ARA&A*, 47, 427
- Hirahara Y., Ohshima Y., Endo Y., 1993, *The Astrophysical Journal Letters*, 403, L83
- Jiménez-Serra I., et al., 2016, *The Astrophysical Journal Letters*, 830, L6
- Jørgensen J. K., et al., 2016, *A&A*, 595, A117
- Kawaguchi K., Ohishi M., Ishikawa S.-I., Kaifu N., 1992a, *The Astrophysical Journal*, 386, L51
- Kawaguchi K., et al., 1992b, *ApJ*, 396, L49
- Kawaguchi K., Kasai Y., Ishikawa S.-I., Ohishi M., Kaifu N., Amano T., 1994, *The Astrophysical Journal Letters*, 420, L95
- Keto E., Rawlings J., Caselli P., 2014, *Monthly Notices of the Royal Astronomical Society*, 440, 2616
- Krüger M., Dreizler H., Preugschat D., Lentz D., 1991, *Angew. Chem. Int. Ed.*, 30, 1644
- Krüger M., Stahl W., Dreizler H., 1993, *J. Mol. Spectrosc.*, 158, 298
- Osamura Y., Fukuzawa K., Terzieva R., Herbst E., 1999, *The Astrophysical Journal*, 519, 697
- Pickett H. M., Poynter R. L., Cohen E. A., Delitsky M. L., Pearson J. C., Müller H. S. P., 1998, *Journal of Quantitative Spectroscopy and Radiative Transfer*, 60, 883
- Quénard D., Vastel C., Ceccarelli C., Hily-Blant P., Lefloch B., Bachiller R., 2017, *MNRAS*, 470, 3194
- Ruud M., Wakelam V., Hersant F., 2016, *Monthly Notices of the Royal Astronomical Society*, pp 3756–3767
- Spezzano S., et al., 2013, *The Astrophysical Journal Letters*, 769, L19
- Suzuki H., Yamamoto S., Ohishi M., Kaifu N., Ishikawa S.-I., Hirahara Y., Takano S., 1992, *The Astrophysical Journal*, 392, 551
- Takano S., et al., 1998, *Astronomy and Astrophysics*, 329, 1156
- Vastel C., Caselli P., Ceccarelli C., Phillips T., Wiedner M. C., Peng R., Houde M., Dominik C., 2006, *The Astrophysical Journal*, 645, 1198
- Vastel C., Ceccarelli C., Lefloch B., Bachiller R., 2014, *The Astrophysical Journal Letters*, 795, L2
- Vastel C., Bottinelli S., Caux E., Glorian J.-M., Boiziot M., 2015a, in SF2A proceedings. pp 313–316, <http://sf2a.eu/proceedings/2015/2015sf2a.conf..0313V.pdf>
- Vastel C., Yamamoto S., Lefloch B., Bachiller R., 2015b, *Astronomy and Astrophysics*, 582, L3
- Vigren E., et al., 2012, *Planetary and Space Science*, 60, 102

## APPENDIX A: SUPPLEMENTARY TABLES

**Table A1.** Quantum numbers  $J$  and  $F$  and observed or calculated<sup>a</sup> transition frequency (MHz) of iminopropadienyli-dene, HNC<sub>3</sub>, up to 50 GHz with consideration of <sup>14</sup>N HFS, their uncertainty<sup>b</sup> Unc. (in kHz) and residual O–C (in kHz) between observed frequency and that calculated from the final set of spectroscopic parameters.

| $J' - J''$ | $F' - F''$ | Frequency              | Unc. | O–C      |
|------------|------------|------------------------|------|----------|
| 1 – 0      | 0 – 1      | 9336.130               | 5.   | 4.71     |
| 1 – 0      | 2 – 1      | 9336.616               | 5.   | 1.33     |
| 1 – 0      | 1 – 1      | 9336.945               | 5.   | 4.08     |
| 2 – 1      | 1 – 1      | 18672.778              | 5.   | –1.49    |
| 2 – 1      | 1 – 2      | 18673.1057             | 1.8  | <i>d</i> |
| 2 – 1      | 3 – 2      | 18673.303              | 5.   | 3.06     |
| 2 – 1      | 2 – 1      | 18673.3232             | 1.5  | <i>d</i> |
| 2 – 1      | 1 – 0      | 18673.598              | 5.   | 2.88     |
| 2 – 1      | 2 – 2      | 18673.675 <sup>c</sup> | 5.   | 25.51    |
| 3 – 2      | 2 – 2      | 28009.4584             | 3.4  | <i>d</i> |
| 3 – 2      | 2 – 3      | 28009.8079             | 2.3  | <i>d</i> |
| 3 – 2      | 4 – 3      | 28009.9348             | 2.3  | <i>d</i> |
| 3 – 2      | 3 – 2      | 28009.9477             | 2.3  | <i>d</i> |
| 3 – 2      | 2 – 1      | 28010.0021             | 2.4  | <i>d</i> |
| 3 – 2      | 3 – 3      | 28010.2973             | 3.3  | <i>d</i> |
| 4 – 3      | 3 – 3      | 37346.0616             | 3.8  | <i>d</i> |
| 4 – 3      | 3 – 4      | 37346.4241             | 3.0  | <i>d</i> |
| 4 – 3      | 5 – 4      | 37346.5195             | 3.0  | <i>d</i> |
| 4 – 3      | 4 – 3      | 37346.5277             | 3.1  | <i>d</i> |
| 4 – 3      | 3 – 2      | 37346.5510             | 3.1  | <i>d</i> |
| 4 – 3      | 4 – 4      | 37346.8902             | 4.0  | <i>d</i> |
| 5 – 4      | 4 – 4      | 46682.5952             | 4.2  | <i>d</i> |
| 5 – 4      | 6 – 5      | 46683.0426             | 3.8  | <i>d</i> |
| 5 – 4      | 5 – 4      | 46683.0483             | 3.8  | <i>d</i> |
| 5 – 4      | 4 – 3      | 46683.0612             | 3.8  | <i>d</i> |
| 5 – 4      | 5 – 5      | 46683.4190             | 4.6  | <i>d</i> |

<sup>a</sup> Frequencies and uncertainties with residuals O–C are experimental ones; those without were calculated from the final set of spectroscopic parameters. <sup>b</sup> 1  $\sigma$  values. <sup>c</sup> Weak line, frequency omitted because of large residual. <sup>d</sup> Calculated frequency and uncertainty.

## APPENDIX B: SUPPLEMENTARY FIGURES

This paper has been typeset from a  $\text{\TeX}/\text{\LaTeX}$  file prepared by the author.

**Table A2.** Quantum numbers  $J$  and  $F$  and observed or calculated<sup>a</sup> transition frequency (MHz) of iminopropadienyli-dene, HNC<sub>3</sub>, up to 300 GHz without consideration of <sup>14</sup>N HFS, their uncertainty<sup>b</sup> Unc. (in kHz) and residual O–C (in kHz) between observed frequency and that calculated from the final set of spectroscopic parameters.

| $J' - J''$ | Frequency   | Unc. | O–C          |
|------------|-------------|------|--------------|
| 1 – 0      | 9336.6690   | 0.8  | <sup>c</sup> |
| 2 – 1      | 18673.3232  | 1.5  | <sup>c</sup> |
| 3 – 2      | 28009.9477  | 2.3  | <sup>c</sup> |
| 4 – 3      | 37346.5277  | 3.1  | <sup>c</sup> |
| 5 – 4      | 46683.0483  | 3.8  | <sup>c</sup> |
| 6 – 5      | 56019.4947  | 4.5  | <sup>c</sup> |
| 7 – 6      | 65355.8519  | 5.1  | <sup>c</sup> |
| 8 – 7      | 74692.1053  | 5.7  | <sup>c</sup> |
| 9 – 8      | 84028.2399  | 6.3  | <sup>c</sup> |
| 10 – 9     | 93364.2409  | 6.8  | <sup>c</sup> |
| 11 – 10    | 102700.0934 | 7.2  | <sup>c</sup> |
| 12 – 11    | 112035.7826 | 7.6  | <sup>c</sup> |
| 13 – 12    | 121371.2937 | 7.9  | <sup>c</sup> |
| 14 – 13    | 130706.6118 | 8.1  | <sup>c</sup> |
| 15 – 14    | 140041.7221 | 8.3  | <sup>c</sup> |
| 16 – 15    | 149376.560  | 25.  | –49.62       |
| 17 – 16    | 158711.2597 | 8.4  | <sup>c</sup> |
| 18 – 17    | 168045.656  | 25.  | –1.31        |
| 19 – 18    | 177379.801  | 25.  | 13.25        |
| 20 – 19    | 186713.634  | 25.  | –2.12        |
| 21 – 20    | 196047.188  | 25.  | 0.43         |
| 22 – 21    | 205380.427  | 25.  | –0.27        |
| 23 – 22    | 214713.3404 | 7.1  | <sup>c</sup> |
| 24 – 23    | 224045.9120 | 7.0  | <sup>c</sup> |
| 25 – 24    | 233378.159  | 25.  | 31.65        |
| 26 – 25    | 242709.925  | 25.  | –46.55       |
| 27 – 26    | 252041.460  | 25.  | 30.23        |
| 28 – 27    | 261372.472  | 25.  | –15.16       |
| 29 – 28    | 270703.119  | 25.  | –9.86        |
| 30 – 29    | 280033.334  | 25.  | –6.05        |
| 31 – 30    | 289363.126  | 25.  | 20.14        |
| 32 – 31    | 298692.4115 | 15.8 | <sup>c</sup> |

<sup>a</sup> Frequencies and uncertainties with residuals O–C are experimental ones; those without were calculated from the final set of spectroscopic parameters. <sup>b</sup> 1  $\sigma$  values. <sup>c</sup> Calculated frequency and uncertainty.

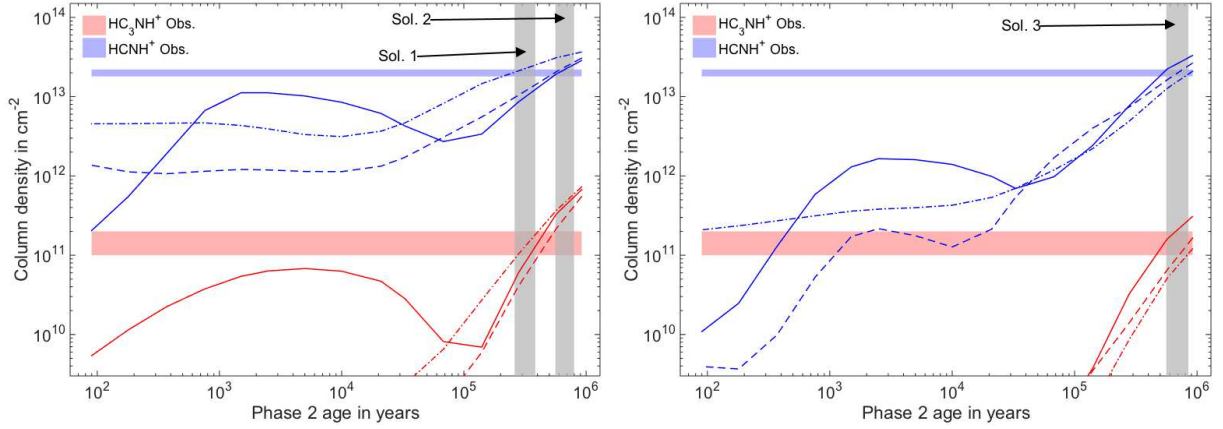


**Figure B1.** Column densities for  $\text{HC}_3\text{NH}^+$ , and  $\text{HCNH}^+$  as a function of the age of the phase 2 for different initial gas densities of the ambient cloud phase:  $10^2 \text{ cm}^{-3}$  (full line),  $3 \times 10^3 \text{ cm}^{-3}$  (dashed line), and  $2 \times 10^4 \text{ cm}^{-3}$  (dash-dotted line). The area of confidence of the observed column densities for these species is also shown. Grey areas shows the timespan area of confidence of each model based on the observed  $\text{HCNH}^+$ . These areas are labelled solutions 1, 2 and 3 (Quénard et al. 2017). *Left panel:* Model EA1 of initial atomic abundances (“low-metal abundances”). *Right panel:* Model EA2 of initial atomic abundances (“high-metal abundances”). All the informations on the modelling can be found in Quénard et al. (2017).

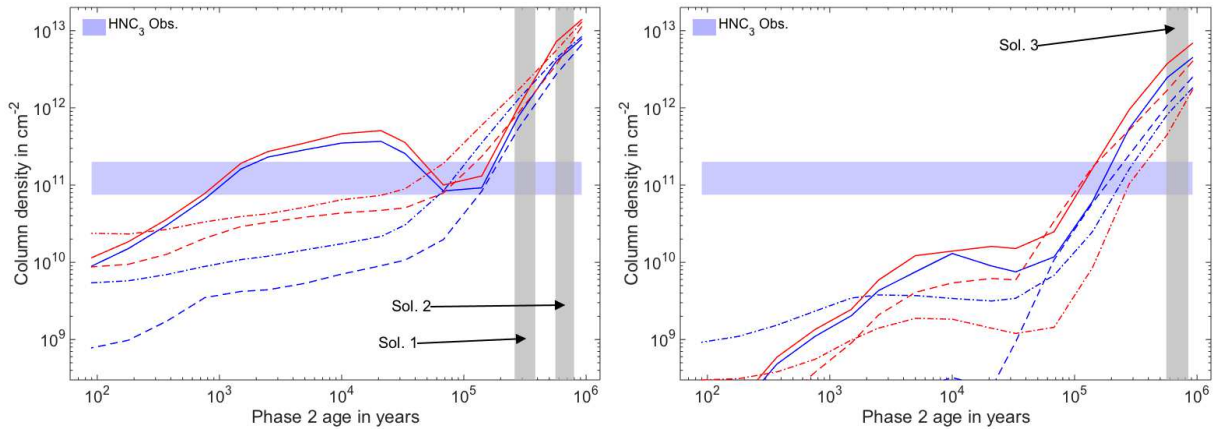


**Figure B2.** Column densities for  $\text{HNC}_3$  as a function of the age of the phase 2 for different initial gas densities of the ambient cloud phase:  $10^2 \text{ cm}^{-3}$  (full line),  $3 \times 10^3 \text{ cm}^{-3}$  (dashed line), and  $2 \times 10^4 \text{ cm}^{-3}$  (dash-dotted line). The red lines correspond to the chemical modelling from Quénard et al. (2017) while the blue lines correspond to the modified network explained in this paper. The area of confidence of the observed column densities for these species is also shown. Grey areas shows the timespan area of confidence of each model based on the observed  $\text{HCNH}^+$ . These areas are labelled solutions 1, 2 and 3 (Quénard et al. 2017). *Left panel:* Model EA1 of initial atomic abundances (“low-metal abundances”). *Right panel:* Model EA2 of initial atomic abundances (“high-metal abundances”). All the informations on the modelling can be found in Quénard et al. (2017).